

Numerical solution of thermal non-Newtonian EHL line contact problem by using preconditioned Newton-GMRES

Mahesh Kumar N^{1*}, Vishwanath B. Awati² and Parashuram M. Obannavar³

^{1*}Assistant Professor,
Department of Mathematics,
Rani Channamma University, Belagavi-591156. Karnataka,India.

²Professor,
Department of Mathematics,
Rani Channamma University, Belagavi-591156. Karnataka,India.

³Research Scholar,
Department of Mathematics,
Rani Channamma University, Belagavi-591156. Karnataka,India.

ABSTRACT

The paper presents, the numerical investigation of thermal Reynolds-Eyring equation for line contact elastohydrodynamic lubrication (EHL). The mathematical modeling of the governing problem involves Reynolds, film thickness, load balance and energy equations with relevant boundary conditions. The governing systems of nonlinear coupled equations are discretized by using finite difference approximations and are solved by using preconditioned Newton-GMRES method consisting of Daubechies D6 wavelets along with multi-level multi-integration (MLMI) technique. The numerical solutions of non-Newtonian EHL line contact with low and high loads for different resolution levels are obtained. The pressure profile and film thickness profile for various loads and resolution levels are predicted in terms of graphs. The present method validates the essential feature of EHL problems and it requires less computer memory space as compared to other numerical schemes. Also, the convergence of the proposed method is much faster than other pure numerical methods. The resulting numerical solutions are compared with earlier findings and are comparable.

KEYWORDS: Thermal EHL, Ree-Eyring model, MLMI, preconditioner.

AMS Subject Classification: 05C12.

Date of Submission: 02-04-2024

Date of acceptance: 13-04-2024

I. INTRODUCTION

The elastohydrodynamic lubrication theory concerns with lubricated film thickness, pressure and elastic deformation of contacting surfaces between non-conformal solid surfaces which comes into contact in presence of lubricants. The elastic deformations of surfaces due to pressure generation in the contact zone which is so high are considered and determined the pressure and lubricant film thickness distributions. These contacts arise in mechanical components such as rollers, gears, bearings, cams etc. due to high pressure generated within the contact zone. Grubin and Vinogradova[1], Dowson and Higginson [2, 3] were pioneers to obtain the numerical solution of EHL problems for Newtonian fluids. Many research investigators have used various numerical methods for considering loads from low to moderate and sliding speeds are obtained, for both film thicknesses and pressure distributions in the case of Newtonian fluids. However, at high load and strain, a large discrepancy arises between experimental and numerical results in case of Newtonian fluid models. To overcome these discrepancies a various non-Newtonian rheological models are available in literature and which are different from Newtonian viscosity law.

The influence of lubricant rheological fluid model was first considered by Bell [4] on film thickness and derived a generalized Reynolds equation for non-Newtonian fluid of Eyring [5] model over pure rolling conditions. The analytical approximations were used to obtain an Ertel-type solution; it predicts that non-Newtonian behavior on film thickness for pure rolling conditions is remarkably influenced. Also, the

experimental data were based on Ertel theory and analytical results for various characteristic behaviors of non-Newtonian fluids. An isothermal EHD line contact with a Ree-Eyring lubricant with pure rolling conditions was analyzed by Kodnir et al. [6]. The author obtained numerical solution of EHD problem initiated with Bell's Reynolds equation and depict the pressure profiles in the form of semi-elliptical with cut-off shape in the outlet region.

The power-law model was introduced by Dyson and Wilson [7] and predicted that shear stress, shear strain profiles decreases in the slope as shear rate increases. The loss of viscosity in shear thinning process was obtained by Hirst and Moore [8] using Eyring's equation [9] and Ree and Eyring [5]. Johnson and Tevaarwerk [10] introduced a nonlinear Maxwell rheological model for lubricant under isothermal conditions, where the total shear strain rate is the sum of an elastic term and nonlinear viscous term is based on Eyring's theory of viscosity. Bair and Winer [11] determined Maxwell rheological model and correlated with experiment results. This model further utilized to determine Ertel-type solutions of EHD problems by Gecim and Winer[12]. The simplified limiting shear stress model was employed to obtain numerical solution of EHD by Jacobson and Hamrock [13]. The results shows that, a reduction in film thickness on Newtonian model when sliding cases were involved. Based on Eyring theory of non-Newtonian, Conry et al. [14] derived a new Reynolds equation of one dimensional flow and numerically analyzed EHL line contact problem. The numerical investigation shows that, the reduction of film thickness under combined rolling/sliding conditions due to non-Newtonian effect.

The thermal effect in the solution of EHL line contact problems was presented by Sternlicht et al. [15]. Cheng and Sternlicht [16] analyzed thermal line contact EHL problem by Newton-Raphson method and assuming the constant viscosity across the lubricant fluid film. Murch and Wilson [17] illustrated the variation in minimum film thickness at the inlet flow due to significant influence of thermal effects with high rolling speeds. Ghosh and Hamrock [18] proposed a new minimum film thickness formula for Newtonian lubricant. Sadeghi and Sui [19] discussed the thermal effects in EHL under pure rolling/sliding contacts by Newton-Raphson method and predicted substantial variations in minimum film thickness. Hsu and Lee [20] proposed a new algorithm of line contact EHL problem under pure sliding /rolling with thermal effects. Lee et al. [21] considered the numerical solution of circular contact EHL under rolling /sliding with thermal effects using multilevel and multi-integration method. Many researchers like Salehizadeh and Saka [22], Wolff et al. [23], Wolff and Kubo [24], Yang and Wen [25], Awati et al. [26] have contributed the line/point/circular contact EHL problems with thermal effects.

In most of the research papers, Newton-Raphson method is used to obtain the solution of EHL problems. In this method, the computational complexity increases due to increase in the size of Jacobian matrix. To overcome the complexity, multigrid method (Lubricant et al.[27], Venner[28]) was introduced in order to reduce the computational complexity of the method from $O(n^3)$ to $O(n \log(n))$. In order to enhance the efficiency in computation of EHL problem multigrid method is used. In this case, calculation domain was divided into two parts, where Gauss-Siedal and Jacobi-dipole relaxation methods are applied in the low pressure contact region and high pressure contact regions respectively. In view of Newton-GMRES method, the solutions are obtained using Krylov subspace of a finite dimensions (Saad[29]). The partition of a domain and inversion of Jacobian matrix is not required in this method. Chen [30] demonstrated the method of preconditioning the sparse dense matrix. Ford et al.[31] used restarted Newton-GMRES method with Daubechies D4 [32] discrete wavelet with permutation as pre-conditioner to solve isothermal EHL line contact problem. The authors depict that preconditioned matrix with banded matrix; the computational complexity is reduced further and mainly focused on computational cost in terms of time and number of iterations. Awati and Kumar [33] extended this method for the analysis of EHL line contact with piezo-viscous fluid. Awati et al [34] scrutinized the effect of electric double layer and surface roughness on EHL problem.

In the present study, numerical investigation of non-Newtonian thermal EHL line contact with Ree-Eyring model comprising modified Reynolds, film thickness, load balance and energy equations using restarted preconditioned Newton-GMRES method consisting of D6 Daubechies wavelet. The numerical results are obtained by varying load and speed which are presented in terms of graphs. Also, the computed results and calculation time are compared with previously published results.

II. RHEOLOGICAL MODEL

The EHL problems in reality, the characteristic behavior for most of the fluid exhibit non-Newtonian in nature. To overcome these difficulties several models were presented in literature, among all those models Eyring model is defined as

$$\frac{\partial u}{\partial z} = \frac{\tau_0}{\eta} \sinh\left(\frac{\tau_{xz}}{\tau_0}\right). \quad (1)$$

Johnson and Tevaarwerk [10] considered a nonlinear viscous model for predicting traction and determine the effect of non-Newtonian behavior on pressure, film thickness profiles based on Ree-Eyring model. The modified Reynolds equation according to Conry et al. [14] becomes

$$\frac{\partial}{\partial x} \left\{ \frac{\rho h^3}{12\eta} S_E(x) \frac{\partial p}{\partial x} \right\} = \frac{(u_1 + u_2)}{2} \frac{\partial(\rho h)}{\partial x} \quad (2)$$

The term $S_E(x)$ in Eq. (2) represents the non-Newtonian effect and is given by

$$S_E(x) = \frac{3(\sum \cosh \sum - \sinh \sum)}{\sum^3} \cosh \left(\frac{\tau_m}{\tau_0} \right), \quad (3)$$

where $\sum = \frac{h}{2\tau_0} \frac{\partial p}{\partial x}$ and the mean shear stress becomes

$$\sinh \left(\frac{\tau_m}{\tau_0} \right) = \frac{\eta(u_2 - u_1)}{\tau_0 h} \frac{\sum}{\sinh \sum}, \quad (4)$$

As $\tau_0 \rightarrow \infty$, it leads to \sum tends to zero and $S_E(x) \rightarrow 1$, it shows that Eyring model leads to Newtonian fluid model. The numerical value of $S_E(x)$ is greater than or equal to unity for all values of \sum and τ_m . In case of pure rolling, $\cosh(\tau_m / \tau_0)$ tends to one.

III. GOVERNING EQUATIONS

The one-dimensional modified Reynolds-Ree-Eyring equation in dimensionless form becomes

$$\frac{\partial}{\partial X} \left\{ \bar{\varepsilon} S_E \frac{\partial P}{\partial X} \right\} = \frac{\partial(\bar{\rho} H)}{\partial X}, \quad (5)$$

where $\bar{\varepsilon} = \frac{\bar{\rho} H^3}{\eta \lambda}$, $\bar{\lambda} = \frac{12\eta_0 \bar{u} R^2}{b^3 P_H}$. The dimensionless variables used in the mathematical formulation of the problem are given as

$$X = \frac{x}{b}, \quad \bar{\eta} = \frac{\eta}{\eta_0}, \quad \rho = \frac{\rho}{\rho_0}, \quad P = \frac{P}{P_h}, \quad H = \frac{hR_x}{b}, \quad U = \frac{\eta_0 u_m}{E'R}, \quad W = \frac{w}{E'R_x}, \quad G = \alpha E'.$$

The cavitations condition with respect to governing physical problem becomes

$$P(X_{in}) = 0, \quad \text{and} \quad P = \frac{dP}{dX} = 0 \quad \text{at} \quad X = X_{out}. \quad (6)$$

The Dowson-Higginson [3] density-pressure relation is given as

$$\bar{\rho} = \left[1 + \frac{0.6 \times 10^{-9} P_H P}{1 + 1.7 \times 10^{-9} P_H P} \right] \quad (7)$$

The Roelands viscosity-pressure relation is read as

$$\bar{\eta} = \exp \left[\{ \ln(\eta_0) + 9.67 \} \left[-1 + (1 + 5.1 \times 10^{-9} P_H P)^{\frac{z}{z-1}} \right] \right] \quad (8)$$

where η_0 is the absolute viscosity, $P_H = \frac{P_h}{P_0}$ is maximum Hertzian pressure, $P_0 = 1.98 \times 10^8$ [Pa] and $\frac{z}{z-1}$ is

a pressure-viscosity index characteristic constant of the fluid. The film thickness equation can be written in dimensionless form as

$$H(X) = H_0 + \left(\frac{X^2}{2} \right) - \frac{1}{\pi} \int_{X_{in}}^{X_{out}} P(X') \ln(X - X')^2 dX' \quad (9)$$

The dimensionless load balance equation becomes

$$\int_{X_{in}}^{X_{out}} P(X) dX = \frac{\pi}{2}. \quad (10)$$

The non-dimensional energy equation with lubricant properties such as specific heat, thermal conductivity and thermal expansivity are constants with respect to pressure or temperature (Yang and Wen [25]), and it can be written as

$$\frac{\partial^2 T}{\partial Z^2} = N_{cv} \left(\bar{\rho} \bar{U} \frac{\partial T}{\partial X} \right) + N_{ac} \frac{T}{\rho} \left(\bar{U} \frac{\partial P}{\partial X} \right) - \bar{\eta}^* N_{vd} \left(\frac{\partial \bar{U}}{\partial Z} \right)^2 \quad (11)$$

where $T = \frac{t}{T_0}$, $\bar{U} = \frac{u}{u_m}$, $\bar{Z} = \frac{z}{H}$, $\bar{\eta}^* = \frac{\eta}{\tau}$, $N_{cv} = \left(\frac{c_p \rho_0 E a^3}{\eta_0 k R_x} \right)$, $N_{ac} = \left(\frac{EP_H a^3 D}{k \eta_0 R_x T_0} \right)$, $N_{vd} = \left(\frac{E^2 R_x^2}{k \eta_0 T_0} \right)$.

$$\bar{U} = \bar{U}_a + \frac{P_H a^3 H^2}{R_x^2 E} \frac{\partial P}{\partial X} \left(\eta_2(\bar{Z}) - \frac{\eta_2(1)}{\eta_1(1)} \eta_1(\bar{Z}) \right) + \frac{\bar{U}_b - \bar{U}_a}{\eta_1(1)} \eta_1(\bar{Z}),$$

$$\eta_1(\bar{Z}) = \int_0^{\bar{Z}} \frac{1}{\bar{\eta}^*} d\bar{Z} \quad \text{and} \quad \eta_2(\bar{Z}) = \int_0^{\bar{Z}} \frac{\bar{Z}}{\bar{\eta}^*} d\bar{Z}.$$

The dimensionless boundary conditions for the energy equation becomes

$$T(X, \bar{Z}) = 1, \text{ at } X = -\infty; T(X, 0) = T_a; T(X, H) = T_b, \tag{12}$$

Where T_a and T_b are respectively denotes the lower and upper surface temperatures of solids. The surfaces temperatures for solid a and solid b respectively becomes

$$T_a(X) = \frac{k_f}{\sqrt{\pi \rho_1 c_1 k_1 u_a}} \int_{X_{in}}^X \left(\frac{\partial T}{\partial Z} \right)_{Z=0} \frac{dS}{\sqrt{X-S}} \tag{13}$$

$$T_b(X) = \frac{k_f}{\sqrt{\pi \rho_2 c_2 k_2 u_b}} \int_{X_{in}}^X \left(\frac{\partial T}{\partial Z} \right)_{Z=H} \frac{dS}{\sqrt{X-S}} \tag{14}$$

IV. DISCRETIZATION OF GOVERNING EQUATIONS

The finite difference approximations are used to discretize the Eqns. (5), (6) and (9), with grid size N . The computation domain is $[X_{in}, X_{out}] = [-4, 1.5]$ and cavitation point X_c is calculated during the solution process by taking negative pressure value is equal to zero. The dimensionless Reynolds equation and cavitation conditions are discretized as

$$\frac{\varepsilon_{i-\frac{1}{2}} P_{i-1} - (\varepsilon_{i-\frac{1}{2}} + \varepsilon_{i+\frac{1}{2}}) P_i + \varepsilon_{i+\frac{1}{2}} P_{i+1}}{\Delta X^2} = \frac{\bar{\rho}_i H_i - \bar{\rho}_{i-1} H_{i-1}}{\Delta X}, \tag{15}$$

where $\Delta X = X_i - X_{i-1}$, $\varepsilon_i = \frac{\bar{\rho}_i H_i^3}{\eta_i \lambda} (S_{E_i})$ and $\varepsilon_{i \pm \frac{1}{2}} = \frac{\varepsilon_i + \varepsilon_{i \pm 1}}{2}$,

$$P(X_{in}) = 0 \quad \text{and} \quad \frac{P(X_{out}) - P(X_{out-1})}{\Delta X} = 0. \tag{16}$$

The discretized form of film thickness equation becomes

$$H_i = H_0 + \frac{X_i^2}{2} - \frac{1}{\pi} \sum_{j=1}^{N+1} D_{i,j} P_j, \tag{17}$$

where $D_{i,j} = \left(i - j + \frac{1}{2} \right) \Delta X \left[\ln \left(\left| i - j + \frac{1}{2} \right| \Delta X \right) - 1 \right] - \left(i - j - \frac{1}{2} \right) \Delta X \left[\ln \left(\left| i - j - \frac{1}{2} \right| \Delta X \right) - 1 \right]$,

for $i = 1, 2, \dots, N+1$ and $j = 1, 2, \dots, N+1$. The load balance equation in discretized form as

$$\Delta X \sum_{i=1}^N \left(\frac{P_i + P_{i+1}}{2} \right) - \frac{\pi}{2} = 0. \tag{18}$$

The discretized form of energy equation can be written as

$$\frac{1}{(\Delta \bar{Z})^2} (T_{k-1} - 2T_k + T_{k+1}) = N_{cv} \bar{\rho}_k \bar{U}_k \left(\frac{T_{i,k} - T_{i-1,k}}{\Delta X} \right) + N_{ac} \bar{U} \frac{T_k}{\rho_k} \frac{\partial P}{\partial X} - N_{vd} \bar{\eta}_k^* \left(\frac{\partial \bar{U}}{\partial \bar{Z}} \right)^2, \tag{19}$$

The pressure and temperature convergence criteria is

$$\frac{\sum (P_i^{k+1} - P_i^k)}{\sum P_i^{k+1}} \leq \varepsilon_1 \quad \text{and} \quad \frac{\sum (T_i^{k+1} - T_i^k)}{\sum T_i^{k+1}} \leq \varepsilon_2$$

where $\varepsilon_1 = 1E-4$ and $\varepsilon_2 = 1E-4$ are error tolerance.

V. NUMERICAL SOLUTION

Newton-GMRES method: The system of linear algebraic equations can be written as

$$Ax = b, \tag{20}$$

where A is a non-symmetric dense matrix and is solved by Krylov subspace iterative methods such as Generalized minimum residual(GMRES) method. In general, the convergence of GMRES method for nonlinear problems is very slow due to increase in the grid size n leads to increase in the condition number of A . Thus, we require an efficient method; first, the coefficient matrix A should be preconditioned. This pre-conditioner matrix A converges much faster when GMRES method is used and solution is obtained for any vector. A sparse matrix P constructed by using discrete wavelet transform and used as right pre-conditioner which approximates matrix A in Eqn. (19). After right preconditioning of Eqn. (19) may be written as

$$AP^{-1}y = b, \quad \text{where } y = Px.$$

If matrix P is a good approximation to matrix A , then it converges for less number of iterations with required error tolerance. To approximate a full matrix A , consider a standard Discrete wavelet transform (DWT) comprising D6 or D4 wavelets, the discrete D4 or D6 wavelet transformation with permutations as proposed by Chen[30]. In this article all the results are calculated by using Daubechies D6 wavelets[34].

Let m be the order of compactly supported wavelets with m coefficients $c_0, c_1, c_2, \dots, c_{m-1}$ low pass filter and $\frac{m}{2}$ vanishing moments. The coefficients d_0, d_1, \dots, d_{m-1} high pass filter is derived from c_i by the relation of the form $d_i = (-1)^i c_{m-1-i}$. Also, let $n = 2^L$ and r is positive integer such that $2^r < m$ and $2^{r+1} \geq m$, where L is the resolution level in the Krylov subspace i.e. $L > r > 0$. Let us denote $s = s^{(L)}$ a column vector of A at the wavelet level L and f is a given function. The wavelet transform $W : s \rightarrow w$ is implemented by well-known pyramidal algorithm. The standard pyramidal algorithm transforms the vector $s^{(L)}$ to $w = \left[\left(s^{(r)} \right)^T \left(f^{(r)} \right)^T \left(f^{(r+1)} \right)^T \dots \left(f^{(L-1)} \right)^T \right]^T$, where $s^{(v)}$ and $f^{(v)}$ are of length 2^v , and the overall sum of these lengths is 2^L .

At a typical level v , $s^{(v)}$ and $f^{(v)}$ are the collections of scaling and wavelet coefficients respectively. In matrix form, w can be expressed as

$$w = P_{r+1} W_{r+1} P_{r+2} W_{r+2} \dots P_{L-1} W_{L-1} P_L W_L = W s^{(L)},$$

where $P_v = \begin{pmatrix} \bar{P}_v \\ J_v \end{pmatrix}_{n \times n}$ with permutation matrix \bar{P}_v of size $2^v = 2^L - k_v = n - k_v$, i.e.

$\bar{P}_v = I(1, 3, \dots, 2^v - 1, 2, 4, \dots, 2^v)$, $W_v = \begin{pmatrix} \bar{W}_v \\ J_v \end{pmatrix}_{n \times n}$ with orthogonal(sparse) matrix \bar{W}_v of size $2^v = 2^L - k_v = n - k_v$ and J_v is an identity matrix of size k_v . Here, $k_L = 0$ and $k_v = k_{v+1} + 2^v$ for $v = L-1, \dots, r+1$.

Jacobian matrix to obtain $\tilde{A} = WAW^T$ which results into a finger like pattern is observed and are presented in Figs. 3 and 4 for $n = 257, 513$ after thresholding with error tolerance $1E-4$. Figs. 5 and 6 represent the pattern of Jacobian matrix at the position of convergent solution. The main advantages of DWT with D6 wavelet coefficients together with permutation requires less number iterations in the inner loop as compared to D4 coefficients DWT with permutation, i.e computational cost in terms of time taken to achieve a reasonable accuracy of the solution requires lesser time. Table 1 presents the comparison of CPU time in seconds with Newton-Raphson method, DWTPer with D4 wavelets and DWTPer with D6 wavelets for low, medium and high loads respectively over different grid size N. It is observed that, the computation time required for D6 DWTPer is less as compared to other numerical methods to obtain the required error tolerance. Also, for a particular grid size N it is observed that, the computational time for CPU is almost same for different loads in the calculation domain for constant speed $L=10$.

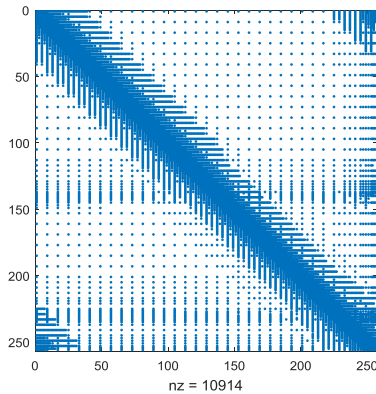


Figure 1. Permutation DWT with D6 wavelets for $n=256$

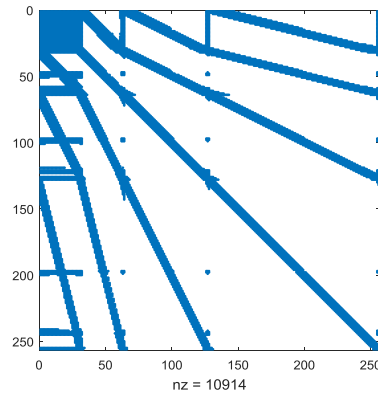


Figure 3. DWT with D6 wavelets for $n=256$

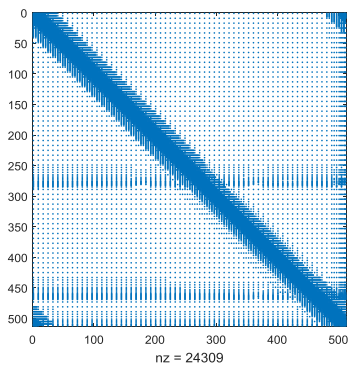


Figure 2. Permutation DWT with D6 wavelets for $n=513$

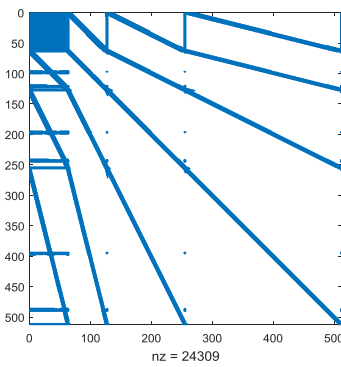


Figure 4. DWT with D6 wavelets for $n=513$

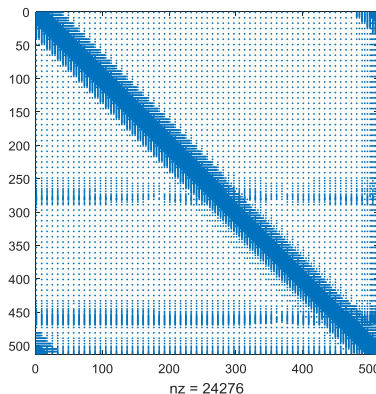


Figure 5. Permutation DWT with D6 wavelets at convergence for $n=513$

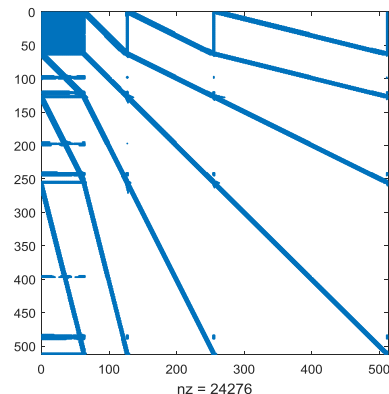


Figure 6. DWT with D6 wavelets at convergence for $n=513$

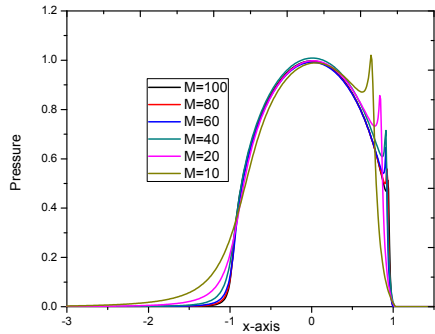


Fig.1 Distribution pressure profiles for various values of M at L=11

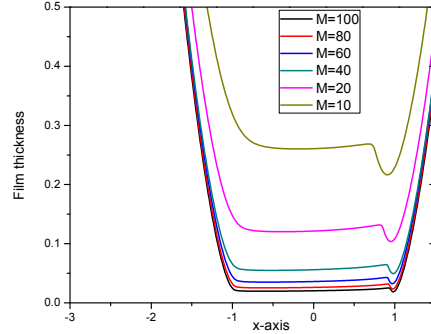


Fig Distribution of film thickness profiles for various values of M at L=11

Figure 7. Distribution of pressure and film thickness profiles for Eyring fluid at various values of M at L=11.

Figure 8. Distribution of pressure and film thickness profiles for Eyring fluid at various values of M at L=11.

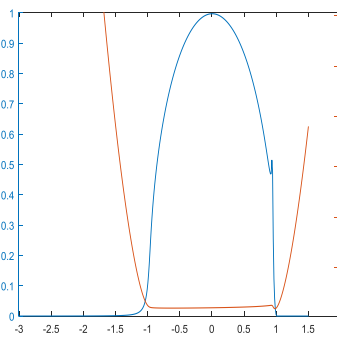


Figure 10. Isothermal Pressure and film thickness profiles for Eyring fluid at M=100 and L=10

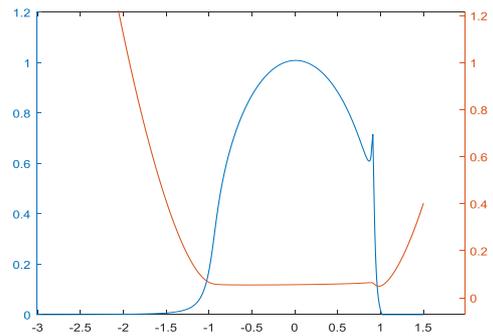


Figure 9. Isothermal Pressure and film thickness profiles for Eyring fluid at M=40 and L=10

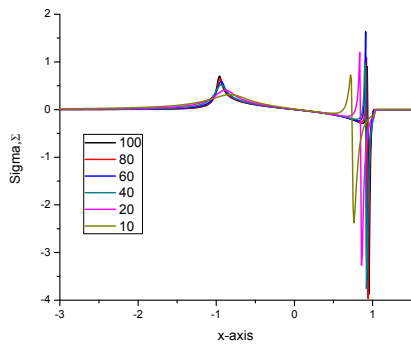


Figure 11. Isothermal sigma profiles for various values of M at L=11.

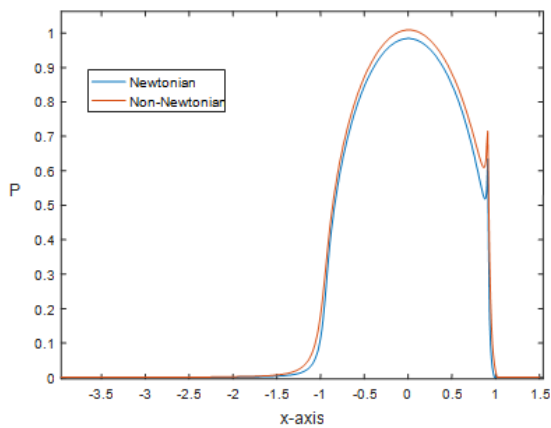


Figure 12. Pressure profiles for M=40 and L=10

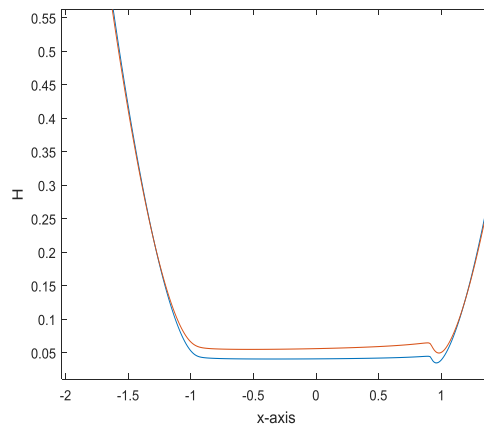


Figure 13. Film thickness profiles for M=40 and L=10

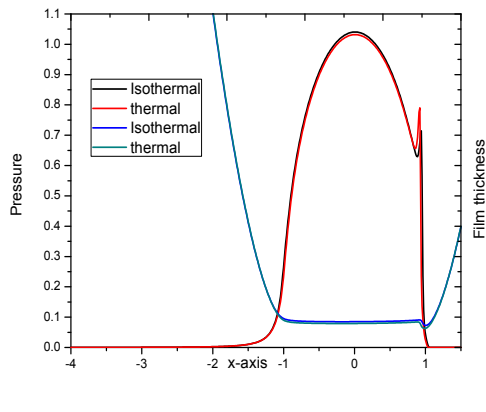


Figure 14. Pressure and film thickness profiles for Eyring fluid at $u_s=2\text{m/s}$ and $w=1e6$.

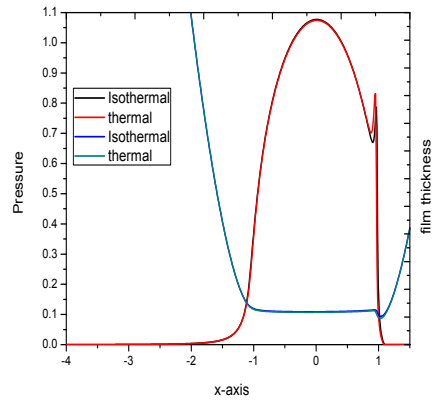


Figure 15. Pressure and film thickness profiles for Eyring fluid at $u_s=3\text{m/s}$ and $w=1e6$.

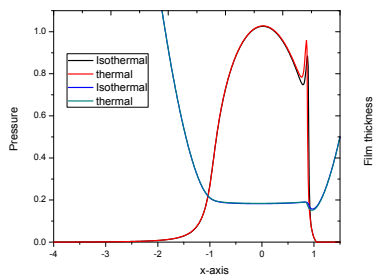


Figure 16. Pressure and film thickness profiles for Eyring fluid at $u_s=2\text{m/s}$ and $w=5e5$.

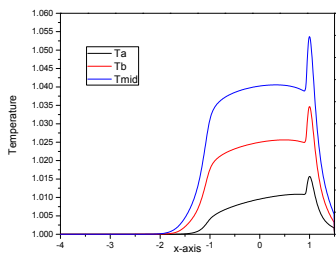


Figure 17. Temperature profiles for Eyring fluid at $u_s=2\text{m/s}$ and $w=1e6$.

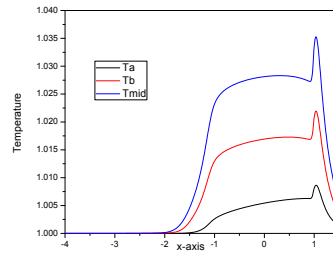


Figure 18. Temperature profiles for Eyring fluid at $u_s=3\text{m/s}$ and $w=1e6$.

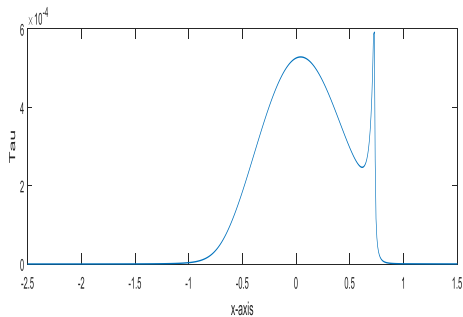


Figure 19. Shear stress profile at $M=10$ and $L=10$.

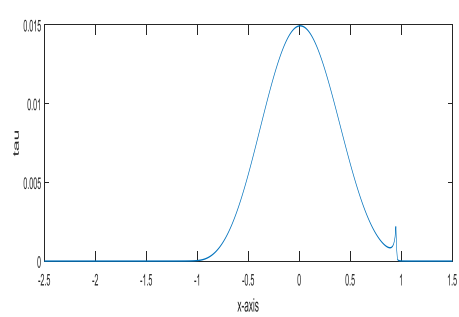


Figure 20. Shear stress profile at $M=20$ and $L=10$.

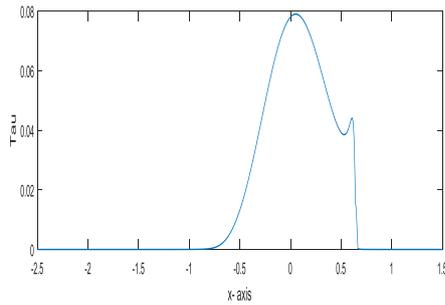


Figure 21. Shear stress profile at M=20 and L=20.

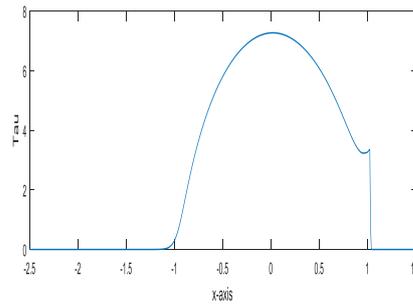


Figure 22. Shear stress profile at M=20 and L=30.

Figs. 7 to 8 determines the pressure and film thickness distributions for different loads M=10, 40, 60, 80 and 100 respectively, at constant speed L=10. It predicts that, increase in M, pressure spike decreases and minimum film thickness also decreases. Figs. 9 and 10 present the isothermal pressure and film thickness profiles for low and high loads at constant speed. Fig. 11 shows the Eyring non-Newtonian characteristics of sigma and in the inlet region for backward flow \sum is slightly increases and decreases, and then there is sudden drop in the \sum profiles as pressure profiles increase in the spike region. Also, the sigma \sum drop value decreases with increase in the value of load. Figs. 12 and 13 shows the difference between isothermal Newtonian and non-Newtonian fluids for pressure and film thickness profiles at M=40 and L=10. It is concluded that, the Newtonian fluid have minimum film thickness as compared to non-Newtonian fluid. Also the height of pressure spike and occurring position decreases for non-Newtonian Eyring fluids as compared with pressure profiles for Newtonian fluids. Figs. 14 to 16 predicts the profiles of isothermal and thermal pressure, film thickness for $u_s=2, 3$ and $w=1E6, 5E5$ respectively. It shows that, the height of pressure spike increases for thermal case, the minimum and central film thickness decreases as compared to isothermal cases. Figs. 17 and 18 determines the temperature profiles consisting of lower, upper and mid layer of lubricants denoted as T_a , T_b and T_{mid} . It shows that, the temperature at middle layer decreases with increasing speed and increases with increase in the loads. Also, the same features are observed in surface temperature. The temperature in middle of the lubricant has higher temperature as compared to boundary layer due to intermolecular forces which results into changes in the viscosity. Also, it is noticed that, temperature profiles increases maximum at the center of the contact region and second maximum is observed near the pressure spike region.

Figs. 19 to 22 represents the plots for τ over the calculation domain for various values of M=5, 10, 20 at L=10 and for different resolution levels for L=20, 25, 30 at M=10 respectively. It depicts that, the increase in M leads to τ increases slightly with a fixed value of L and symmetry or spread of the curve decreases. The curve and spread values of τ increases with an increase in the resolution level L at constant M. Also, it predicts τ exhibit second spike curve due to pressure spike for lower value of L and M, which decreases with increase in load and speed.

VIII. CONCLUSION

The preconditioned Newton-GMRES method with restarted comprising DWT with Daubechies D6 wavelet is an elegant and more efficient numerical method. This method converges much faster and requires less computational time (CPU) as compared to other classical numerical methods. This method can be used as an alternative method for the solution of EHL problems with Newtonian and non-Newtonian fluids. The minimum film thickness of thermal non-Newtonian case decreases as compared to isothermal non-Newtonian cases. Pressure spike increases slightly in thermal effect as compared to isothermal conditions. Also, pressure spike value decreases as compared to Newtonian cases, whereas central and minimum film thickness of non-Newtonian Eyring fluid model increases as compared to Newtonian model.

Acknowledgments: One of authors (MKN) would like to thank Rani Channamma University, Belagavi, India (Ref. No.: RCUB/PMEB/2020-21/41) for the financial support through the award of research grant.

REFERENCES

- [1]. A. N. Grubin, and I. E. Vinogradova, Investigation of the Contact of Machine Components, Central Scientific Research Institute for Technology and Mechanical Engineering, Book No. 30, Moscow (D.S.I.R. Translation, No. 337), 1949.
- [2]. D. Dowson, and G. R. Higginson, A Numerical Solution to the Elastohydrodynamic Problem, J. Mech. Engr. Sci. Volume 11, Number 1 (1959), pp. 7-15.
- [3]. D. Dowson, and G. R. Higginson, Elastohydrodynamic lubrication, the fundamentals of roller and gears lubrication, Pergamon, Oxford, 1966.
- [4]. J. C. Bell, Lubrication of Rolling Surfaces by a Ree-Eyring Fluid, ASLE Transactions. Volume 5, (1962), pp. 160-171.

- [5]. T. Ree, and H. Eyring, Theory of non-Newtonian flow. I. Solid plastic system, and Theory of non-Newtonian flow. II. Solution system of high polymers, *J. Appl. Physics*. Volume 26, Number 7 (1955), pp. 793-800, (Part I) and pp. 800-809 (Part II).
- [6]. D. Kodmir, R. Salikvadze, D. Bakashvili, and V. Schwaetzman, A solution of the elastohydrodynamic problem for non-Newtonian Fluids, *ASME Journal of lubrication technology*. Volume 97, (1975), pp.303-320.
- [7]. A. Dyson, and A. Wilson, Film thickness in elastohydrodynamic lubrication by silicon fluids, *Proc. of the Inst. of Mech. Eng.* Volume 180, (1966), Part 3B, pp. 97-112.
- [8]. W. Hirst, and A. Moore, Non-Newtonian behavior in elastohydrodynamic lubrication, *Proc. Royal Soc., London, Series A*. Volume 337, (1974), pp.101
- [9]. H. Eyring, Viscosity, Plasticity and Diffusion example of absolute reaction rates, *J. Chem. Phys.* Volume 4, (1936), pp. 283-291.
- [10]. K. Johnson, and J. Tevaarwerk, Shear behaviour of EHD Oil Films, *Proc. Royal Soc, London, Series A*. Volume 356, (1977), pp. 215-236.
- [11]. S. Bair, and W. Winer, A Rheological Model for EHL contacts based on primary laboratory data, *ASME Journal of Lubrication Technology*. Volume 101, (1979), pp. 258-265.
- [12]. B. Gecim, and W. Winer, Lubricant limiting shear stress effect on EHD film thickness, *ASME Journal of Lubrication Technology*. Volume 102, (1980), pp. 213.
- [13]. B. O. Jacobson, and B. J. Hamrock, Non-Newtonian behavior in elastohydrodynamic lubrication of rectangular contacts, *ASME Journal of Tribology*. Volume 106, (1984), pp. 275-284.
- [14]. T. Conry, S. Wang, and C. Cusano, A Reynolds-Eyring equation for elastohydrodynamic lubrication in line contacts, *ASME Journal of Tribology*. Volume 109, (1987), pp. 648-658.
- [15]. G. P. Sternlicht, P. Lewis and P. Flynn, Theory of lubrication and failure of rolling contacts. *ASME, Transaction of tribology*. Volume 83, (1961), pp. 213.
- [16]. H. S. Cheng, and B. Sternlicht. A numerical solution for the pressure. temperature and film thickness between two infinitely long, lubricated rolling and sliding cylinders, under heavy loads. *Journal of Basic Engineering* . Volume 103, (1965), pp. 695-707.
- [17]. L. Murch, and W.R.D. Wilson, A thermal elastohydrodynamic inlet zone analysis. *ASME, Journal of Lubrication Technology*. Volume 97, (1975), pp. 212-216.
- [18]. M. K. Ghosh, and B.J. Hamrock, Thermal elastohydrodynamic lubrication of line contacts, *ASLE Transaction*. Volume 28, (1985), pp. 159-171.
- [19]. F. Sadeghi, and P. C. Sui, Thermal elastohydrodynamic lubrication of rolling/sliding contacts, *ASME, Journal of Tribology*. Volume 112, (1990), pp. 189-195.
- [20]. C. Hsu, and R.T. Lee, An efficient algorithm for thermal elastohydrodynamic lubrication under rolling/sliding line contacts, *ASME, Journal of Tribology*. Volume 116, (1994), pp. 762-769.
- [21]. R. T. Lee, C.H. Hsu and W.F. Kuo, Multilevel solution for thermal elastohydrodynamic lubrication of rolling/sliding circular contacts, *Tribology International*. Volume 28, (1995), pp. 541-552.
- [22]. H. Salehizadeh, and N. Saka, Thermal non-Newtonian elastohydrodynamic lubrication of rolling line contacts, *ASME, Journal of Tribology*. Volume 113, (1991), pp. 481-491.
- [23]. R. T. Wolff, A. Nonaka, A. Kubo and K. Matsou, Thermal elastohydrodynamic lubrication of rolling/sliding line contacts. *ASME, Journal of Tribology*. Volume 114, (1992), pp. 706-713.
- [24]. R. T. Wolff, and A. Kubo, The application of Newton-Raphson method to thermal elastohydrodynamic lubrication of line contacts, *ASME. Journal of Tribology*. Volume 116, (1994), pp. 733-740.
- [25]. P. Yang, and S. Wen, A fast, robust, straightforward algorithm for thermal elastohydrodynamic lubrication, *Tribology International*. Volume 26, (1993), pp. 17-23.
- [26]. V. B. Awati, N. Mahesh Kumar and N. B. Bujurke, Numerical solution of thermal EHL line contact with biobased oil as lubricant, *Australian journal of mechanical engineering*. Volume 20, Number 1 (2022), pp. 231-244.
- [27]. A. Lubrecht, T. Napel, and R. Bosma, Multigrid, an alternative method for calculating film thickness and pressure profiles in elastohydrodynamically lubricated line contacts, *Trans. ASME, J. Tribology*. Volume 108, (1986), pp. 551-556.
- [28]. C. H. Venner, Multilevel solution of the EHL line and point contact problems. PhD thesis, University of Twente, The Netherlands.
- [29]. Y. Saad, Iterative methods for sparse linear systems. PWS, Boston, 1996.
- [30]. K. Chen, Discrete wavelet transforms accelerated sparse preconditioners for dense boundary element systems, *Elect. Trans. Numer. Anal.* Volume 8, (1999), pp. 138-153.
- [31]. J. Ford, K. Chen, and L. Scales, A new wavelet transform preconditioner for iterative solution of elastohydrodynamic lubrication problems, *Int. J. Comput. Maths*. Volume 75, (2000), pp. 497-513.
- [32]. I. Daubechies, Ten lectures on wavelets. SIAM, Philadelphia, PA, 1992.
- [33]. V. B. Awati, and N. Mahesh Kumar, Newton-GMRES Method for the solution of Piezo viscous line contact EHL problem with Daubechies wavelet as a preconditioner, *Journal of modern Industry and Manufacturing.*, Volume 1, (2023), pp. 1-8.
- [34]. V. B. Awati, P. M. Obannavar and N. Mahesh Kumar, Newton-GMRES method for the scritinization of electric double layer and surface roughness on EHL line contact problem, *Journal of Mechanical engineering and Sciences*. Volume 17, Number 1, (2023), pp. 9370-9382.